



www.sciencemag.org/cgi/content/full/315/5820/1813/DC1

Supporting Online Material for
**Seismostratigraphy and Thermal Structure
of Earth's Core-Mantle Boundary Region**

R. D. van der Hilst,* M. V. de Hoop, P. Wang, S.-H. Shim, P. Ma, L. Tenorio

*To whom correspondence should be addressed. E-mail: hilst@mit.edu

Published 30 March 2007, *Science* **315**, 1813 (2007)
DOI: 10.1126/science.1137867

This PDF file includes:

SOM Text
Figs. S1 to S3
References

SUPPLEMENTARY ONLINE MATERIAL

Text S1: Method - Inverse scattering

(Seismic) inverse scattering refers to a class of inverse theories used to characterize Earth's structure on scale lengths comparable to or smaller than the wavelengths of the seismic waves used as data. We investigate scatterers (e.g., interfaces) in Earth's lowermost mantle (that is, the core-mantle boundary and the so called D'' region above it) with a generalized Radon transform (GRT) adapted from application to near surface (hydrocarbon reservoir) imaging. A GRT maps singly scattered waves to multiple images (or "common image-point gathers") – for different opening or scatter angles (~ source-receiver distances) – of the same target structure. The theoretical analysis dates back to Guillemin (*S1*), but the first application to seismic waves is credited to Beylkin (*S2*). This early work was done in the context of hydrocarbon reservoir imaging with acoustic waves and in the absence of caustics. Later extensions included anisotropic media (*S3*), resolution analysis (*S4*), and generic elasticity with caustics (*S5*).

The GRT approach used here is presented in Wang *et al.* (*S6*). For imaging of Earth's deep interior we use the broad-band *ScS* wavefield, which contains the specular (that is, mirror-like) core-mantle boundary (CMB) reflections as well as energy that arrives earlier (precursors) and later (coda) due to specular and non-specular reflection at or above the CMB (Fig. 1A). The GRT exploits 3-D data coverage, handles caustics due to mantle heterogeneity, and accounts through careful weighting for variations in wave amplitude due to radiation patterns and geometrical spreading.

A key concept is “data redundancy”, which arises from the sampling of the same image point by scattered waves (that is, specular and non-specular reflections, some arriving as precursors to *ScS*, others in its coda) that can be observed over a wide range of epicentral distances and azimuths. The procedure involves three steps (illustrated in Fig. S2). First, the broad band data are used to construct radial image profiles of the same target structure at a range of opening (or scatter) angles. Second, these “common image point gathers” are used to estimate (using statistical inference, text S2, below) a single profile at a selected CMB location (Fig. S1). Third, lateral juxtaposition of these 1-D reflectivity profiles produces 2-D scatter images of the lowermost mantle.

Text S2: Method - Statistics

Instead of simply stacking the image gathers (short for ‘common image-point gathers’) over different scattering angles (and azimuths) into a single reflectivity profile, we use statistical methods to estimate and enhance the GRT images (*s7*). A key notion of our approach is that noise in the data and the image gathers is allowed to have mixed (that is, white and coherent) components. The correlated components can be due to, for instance, uneven source-receiver distribution, conflicting phases, multiple scattering, and the use of an inaccurate reference model for (3D) mantle wavespeed, and the parameters that control them can be estimated from the image gathers through prediction error minimization (also known as generalized cross-validation).

The estimation procedure is based on penalized least squares (see *s8*, *s9*, *s10* for comprehensive treatments of this subject), also known as (standard) Tikhonov regularization, it is adapted to account for correlated noise through use of ‘mixed-effects’ statistical models (*s11*, *s12*, *s13*). This flexible type of Tikhonov regularization can be used with different types of correlated noise and with sparsely and unevenly sampled image gathers. Along with improved estimates of the reflectivity profile (the image), it also produces rigorous Bayesian confidence bands. These confidence bands replace forward modeling as the initial model validation tool. This allows (routine) application to very large data sets and can be used to focus the interpretation to structures that are imaged at a particular level of confidence.

Text S3: Data

Applications involving the (forward) modeling of waveforms or waveform stacks rely on near or post-critical reflections because only those produce signal at sufficient amplitudes for visual inspection and modeling, see Fig. S1. The narrow distance range in which these very wide angle data are observed ($\sim 74\text{-}85^\circ$, but more often $\sim 79\text{-}82^\circ$) limits the CMB regions that can be studied. Also, the narrow distance window can combine with the uneven source-receiver distribution to leave fairly narrow azimuth ranges from which data can be used. Effectively, this renders a 2-D analysis even when imaging methods themselves are intrinsically 3-D. For instance, for D’’ imaging beneath Central America, near-post critical reflections are mainly observed in data from earthquakes in South

America recorded in North America (that is, a NW-SE direction), which would degrade image sections in SW-NE direction. The inclusion of (relatively) narrow angle data allows sampling of the target from all azimuths.

At angles much smaller than the near critical arrival, the reflection coefficient is small (Fig. S1) and, consequently, the diagnostic signal too weak for direct visual inspection. These angles are, therefore, rarely used in studies based on forward modeling of (stacks of) waveforms. Using data redundancy, the GRT approach extracts signal from data in a wide distance range. We consider data at epicentral distances from 43-80°, with most data between 50-70° (Fig. S3); that is, most of the images are constrained by data that are not used in modeling studies (e.g., *S14*, *S15*). The inclusion of relatively narrow angle data enhances radial resolution, because the pulse width in the image gathers increases (dilates) with increasing angle (Fig. S1), and dramatically improves 3-D data coverage.

We used the transverse-component *ScS* wavefield from 1,500 earthquakes ($m_b > 5.2$, origin time 1988-2006) recorded at one or more of a total of 1,200 seismograph stations. The total number of broad band records used is ~80,000. For all events considered here, origin times and source locations (hypocenters) were obtained from (*S16*) and moment tensors and magnitudes from the Harvard centroid moment tensor (CMT) catalog. For all events in our data set, three-component broadband waveforms were retrieved from the Data Management Center of the Incorporated Research Institutions for Seismology (IRIS). For details of the data processing we refer to Wang *et al.* (*S6*). The most important aspects are: band-pass filtering (accepting periods between 1-20 s), removal of the instrument response to suppress effects of different recording systems, estimation (and removal – by deconvolution – from the data) of the source signature using a polarity check and a principal component analysis, amplitude normalization to the *ScS* reflection avoid predominance of a few large earthquakes, and correction for Earth's ellipticity.

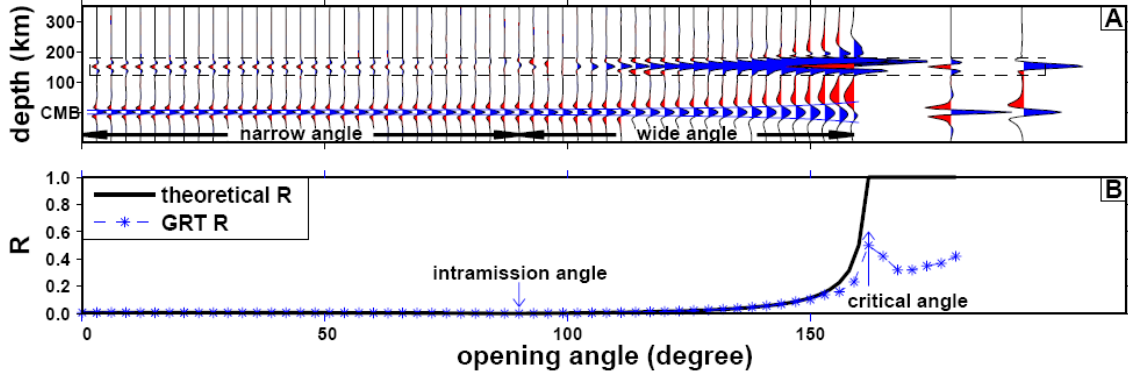


Figure S1. Construction of GRT stacks (images) from image gathers at different scatter (or opening) angle θ with synthetic data calculated from a simple wavespeed model with a velocity increase at 150 km above the core-mantle boundary (S_6). For illustration purposes we used an artificial (regular) source receiver distribution. For specular reflection, the epicentral distance is half the scatter angle θ . (A) The traces on the left are image gathers at 53 scattering angles produced from synthetic data. The traces on the right are stacks over narrow and wide angles. Separate integration over narrow and wide angles is necessary because of the change in polarity upon crossing the intramission angle (here at 46.6°). The pulse-width, or dilation, depends on scatter angle as $1/\cos(\theta/2)$ – the theoretical values are depicted by the thin blue lines around the depth of the CMB. To aid visual inspection, the amplitude in the (dashed) box is amplified by a factor of 20. (B) The solid line gives the theoretical reflection coefficient R calculated and the stars depict R inferred from by the generalized Radon transform. (NB. The GRT can only handle pre-critical reflections.) Sampling at narrow angles provides the best radial resolution (smallest dilation) but the reflection coefficient is small; sampling at wide angles produces a large reflection but has low radial resolution (large dilation). Inverse scattering can extract structural signal from both narrow and wide angle data, yielding superior data coverage and radial resolution, whereas forward modeling relies solely on reflections close to (or beyond) the critical angle.

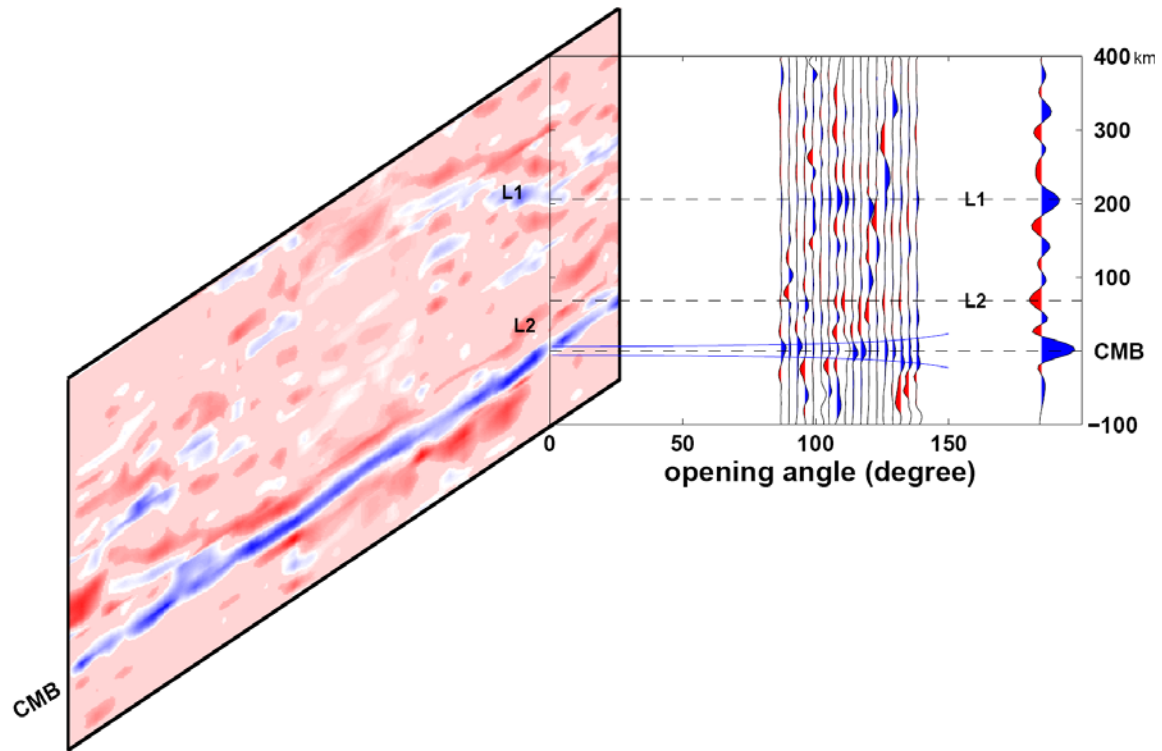


Figure S2. From image gathers at specific angles to radial GRT profiles to 2-D scattering sections. On the right we show common image point gathers in (scatter, or opening) angle for a selected image point at the core-mantle boundary (CMB); to the right of these gathers we show the generalized Radon transform (GRT) trace, which represents an image of the radial contrasts in elasticity and density at that CMB point. On the left we show a 2-D image profile (B-B' in Figs. 1-3) that results from juxtaposition of (and linear interpolation between) 40 of such GRT images. Peaks in contrast associated with a positive reflection coefficient produce blue 'events' in the seismic sections, for instance interface L1; negative reflection coefficients produce red 'events', for instance interface L2. We emphasize that the radial GRT profiles are not produced by simple stacking of the images gathers at specific angles but that the best estimates of them are obtained by mixed-effect model statistics (S7).

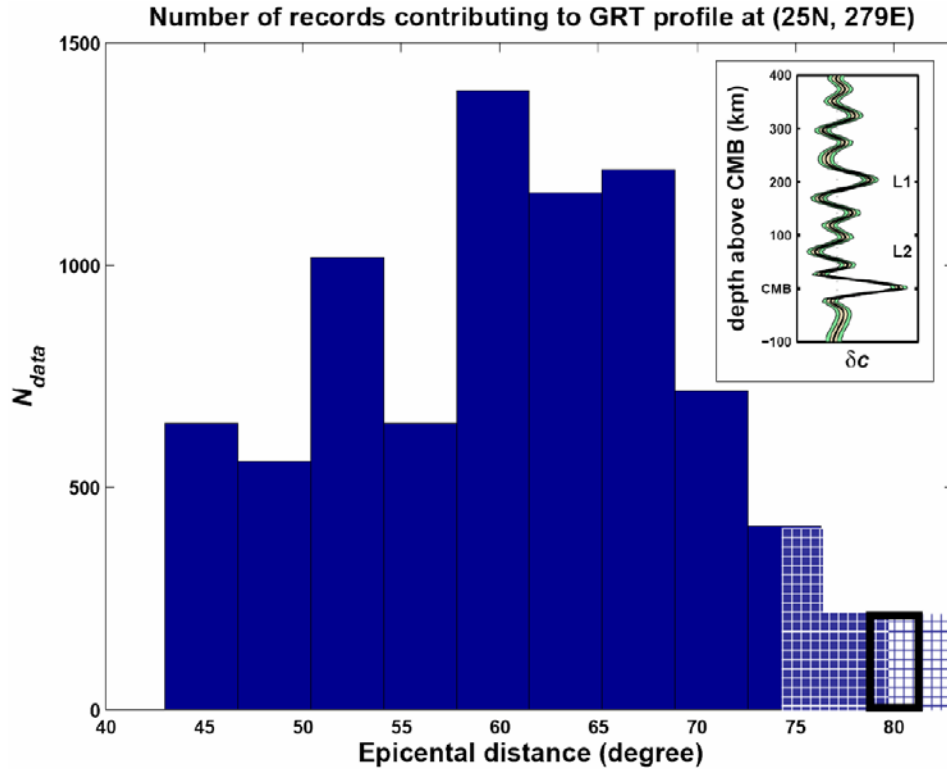


Figure S3. Number of (broad-band) records contributing to the construction – through the GRT – of a radial reflectivity profile (inset, top right) at geographical location (25°N, 279°E), which is along Section B-B' (Fig. 1). The full range considered in the GRT is 43°-80°, but most of the data are associated with epicentral distances between 50° and 72°. (We note that for other image points the distance distribution may be different.) For comparison, studies that rely on modeling of waveforms or stacks commonly use data in a narrow distance range (~74-85°, shaded, but more often ~79-82°, fat rectangle) where near critical arrivals are observed. In the radial profile (inset) the 1σ (68%) level is marked in grey/yellow and the 2σ (95%) confidence band is depicted in green around the average (thin black line). Structures L1 and L2 are still significant at the 2σ level.

References cited in Supplementary Online Material:

- S1. V. Guillemin, *Proc. Symp. Pure Math.* **43** (1985).
- S2. G. Beylkin, *J. of Math. Phys.* **26**, 99 (1985).
- S3. R. Burridge *et al.*, *Geoph. J. Int.* **134**, 757 (1998).
- S4. M.V. de Hoop *et al.*, *Geophysics* **64**, 852 (1999).
- S5. C. Stolk, M.V. de Hoop, *Comm. Pure Appl. Math.* **55**, 261 (2006).
- S6. P. Wang, M.V. de Hoop, R.D. van der Hilst, P. Ma, and L. Tenorio, *J. Geophys. Res.*, **111**, doi:10.1029/2005JB004241 (2006).
- S7. P. Ma, P. Wang, M.V. de Hoop, L. Tenorio, and R.D. van der Hilst, *J. Geophys. Res.*, in press (<http://quake.mit.edu/hilstgroup/robepage/PapersPDF/2006JB004513R.pdf>).
- S8. Wahba, G., *CBMF-NSF Regional Conference Series in Applied Mathematics*, **59**, Soc. Industr. Appl. Math., 1990.
- S9. Gu, C., *Smoothing spline ANOVA models* (Springer-Verlag, New York, 2002).
- S10. Tenorio, L., *Soc. Indust. Appl. Math. Review*, **43**, 347 (2001).
- S11. Vonesh, E.F., Chinchilli, V.M., *Linear and nonlinear models for the analysis of repeated measurements* (Marcel Dekker Inc., New York, 560 pp., 1997).
- S12. Gu, C., Ma, P., *Ann. Stat.*, **33**, 1357 (2005).
- S13. Pinheiro, J.C., Bates, D.M., *Mixed effects models in S and S-plus* (Springer-Verlag, New York, xvi+528 pp., 2000).
- S14. T. Lay, J. Hernlund, E. J. Garnero, M. S. Thorne, *Science* **314**, 1272 (2006).
- S15. A. Hutko, T. Lay, E. J. Garnero, J. Revenaugh, *Nature* **441**, 333 (2006).
- S16. E.R. Engdahl, R.D. van der Hilst, R.P. Buland, *Bull. Seism. Soc. Am.* **88**, 722-743 (1998).